Available online at www.sciencedirect.com
SCIENCE DIRECT®
Physics of the Earth and Planetary Interiors 151 (2005) 53–76
PHYSICS OF THE EARTH AND PLANETARY INTERIORS
www.elsevier.com/locate/pepi

Subevent analysis for the Tabas earthquake of September 16, 1978, using near field accelerograms

I. Sarkar [a,*], V. SriRam [b], H. Hamzehloo [c], K.N. Khattri [d]

[a] *Department of Earth Sciences, Indian Institute of Technology, Roorkee 247 667, India*
[b] *Wadia Institute of Himalayan Geology, Dehra Dun 248001, India*
[c] *International Institute of Earthquake Engineering and Seismology, Tehran, I.R., Iran*
[d] *100 Rajendra Nagar, Kaulagarh Road, Dehra Dun 248001, India*

Received 7 May 2004; received in revised form 8 October 2004; accepted 11 January 2005

Abstract

We analyze the strong motion accelerograms of the large magnitude ($m_b = 6.4$, $M_S = 7.7$, $M_w = 7.4$, $M_0 = 1.32 \times 10^{20}$) Tabas earthquake of September 16, 1978. The earthquake occurred due to a unilaterally propagating complex rupture process on a thrust fault system. The imprints of rupture of four (and possibly five) asperities (sub-faults) have been identified on the accelerograms. Using derived 'SH-wave' records, the locations of these asperities, which lie on the main causative fault, and the relative times of their occurrence have been determined. A foreshock that occurred about 6 s prior to the main shock has also been identified and located. Further, using 'SH-wave' spectral data, we provide near field estimates of the strike, dip and slip of these asperities as well as their seismic moment, moment magnitude, fault area, released shear wave energy and average stress drop. The spectra of the sub-events conform to the ω^{-2} Brune spectra. The total seismic energy of the sub-events is consistent with the radiated energy estimated from teleseismic observations. The fault plane solutions show generally WNW–ESE strike, which is sub-parallel to the regional strike of the geological fault system existing in the area. The stress drops are in the range of 7–30 bar, with the exception of the main sub-event that showed a stress drop of 100 bar. Overall the sub-events show self-similarity. The average shear wave quality factor Q_S, which in the near field is quite sensitive to the local site geology, has been found to lie between 600 and 1200. The decay of PGA with distance is found to be compatible with Niazi and Bozorgnia's [Niazi, M., Bozorgnia, Y., 1992. The 1990 Manjil, Iran earthquake: geology and seismological overview, PGA attenuation and observed damage. Bull. Seism. Soc. Am. 82, 774–799] attenuation relation for the region.

Keywords: Transverse accelerograms; Asperities; Source parameters; QS

* Corresponding author. Tel.: +91 1332 285560; fax: +91 1332 285638.
E-mail addresses: irenefes@iitr.ernet.in (I. Sarkar), sriramvi@rediffmail.com (V. SriRam), hhamzehloo@dena.iiees.ac.ir (H. Hamzehloo), knkhattri@hotmail.com (K.N. Khattri).

0031-9201/$ – see front matter © 2005 Elsevier B.V. All rights reserved.
doi:10.1016/j.pepi.2005.01.004

1. Introduction

The large magnitude ($m_b = 6.4$, $M_S = 7.7$, $M_w = 7.4$, $M_0 = 1.32 \times 10^{20}$) Tabas earthquake that occurred on September 16, 1978, 15:35:56 UT, in the Khorassan province of east central Iran (Fig. 1a), is considered to be one of the most destructive regional events of the 20th century. It completely destroyed the oasis town of Tabas, killed more than 85% of its inhabitants and also caused intense havoc and destruction to the life and property of the inhabitants of several other neighboring towns and villages. According to damage survey reports, more than 20,000 people were killed, thousands were injured and more than 15,000 houses were destroyed in this disaster (Mohajer-Ashjai and Nowroozi, 1979; Berbarian et al., 1979; Berbarian, 1982).

Compared to the high rate of deformation and intense seismic activity observed in the Zagros mountain

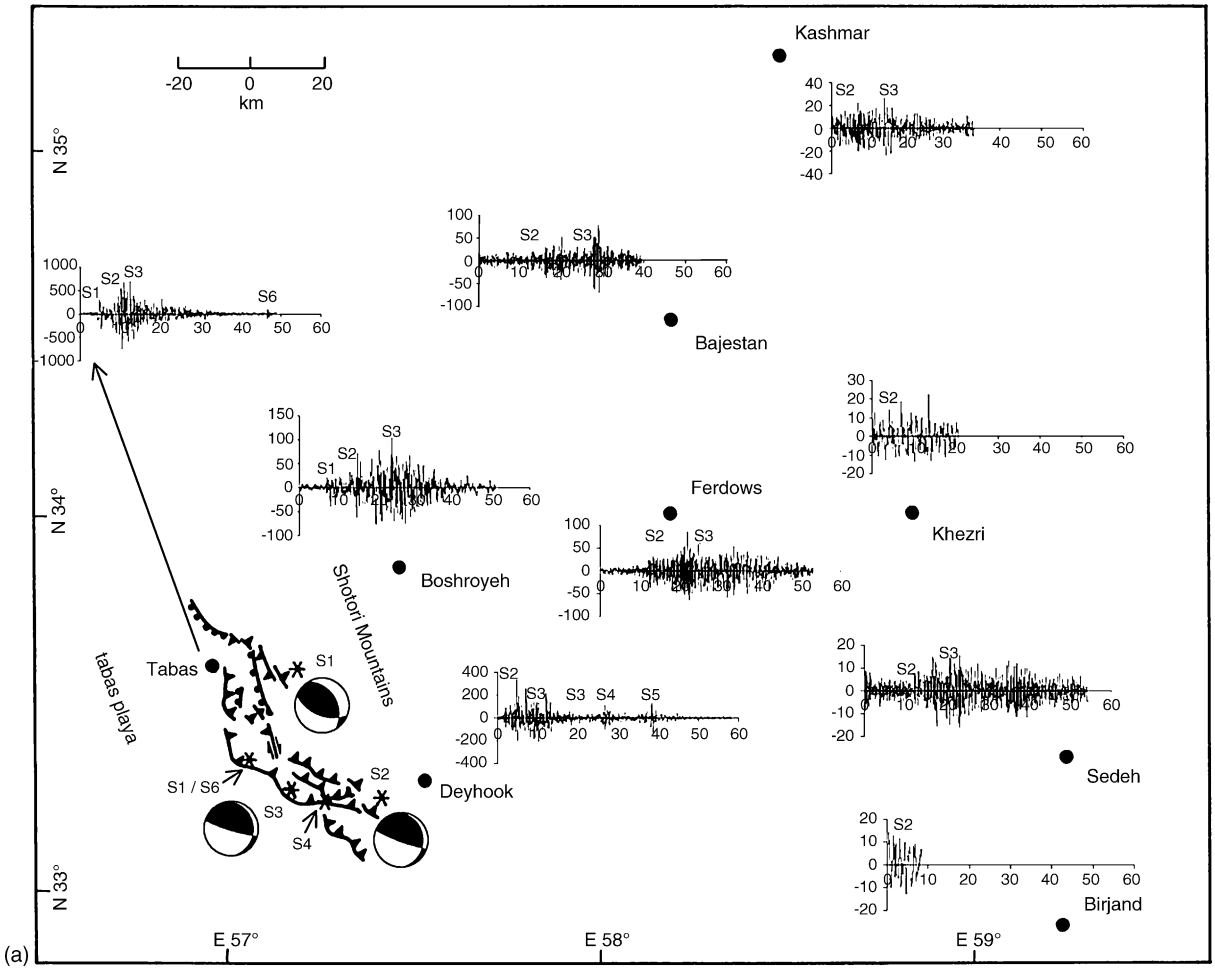

Fig. 1. (a) Map of the Tabas earthquake epicentral area. The locations of the surface ruptures are adapted from Berbarian et al. (1979). The closed circles mark the locations of the nine strong motion stations whose data is analyzed in this study. The derived transverse wave accelerograms for the main burst of energy (see text and (b)) are shown alongside the corresponding stations. Here the horizontal axis denotes time in seconds; the vertical axis denotes the acceleration in cm/s^2. The epicentral locations of the five sub events (marked with asterisks) and fault plane solutions of three of these, as estimated in the study, are also shown. (b) The transverse accelerograms ('SH-wave' accelerograms') for the main burst of energy, derived from rotating the horizontal accelerograms through the back azimuth angles from the S2 epicenter to the nine accelerograph stations (see text and also (a) and the corresponding velocity seismograms, are shown here. The six strong phases of energy release are identified distinctly on these accelerograms and the corresponding velocity seismograms.

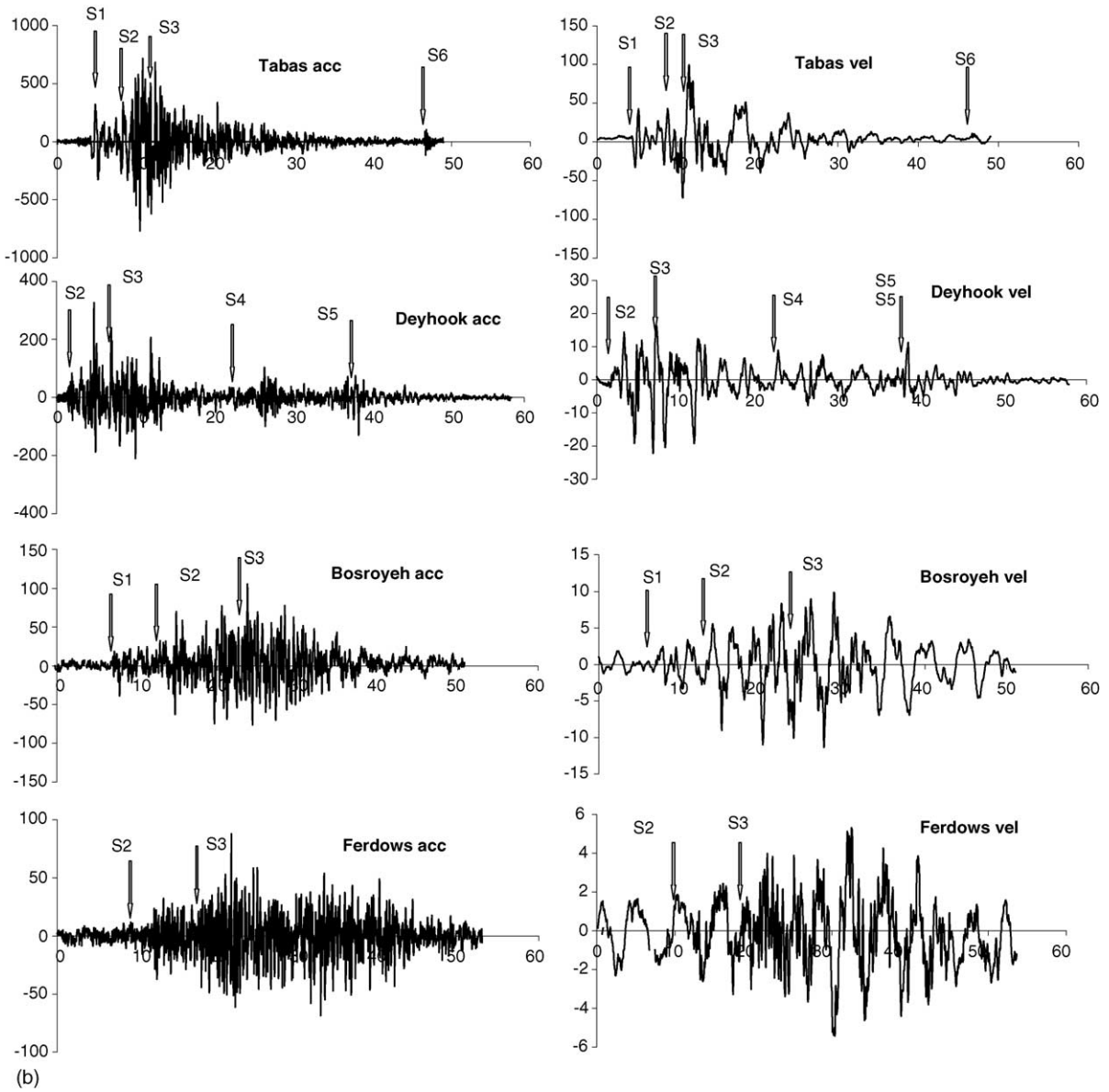

Fig. 1. (*Continued*)

ranges in southern Iran and Alborz and Kopeh Dagh mountain ranges in northern Iran, the central Iran block and the Lut block to its southeast are generally considered to be undeforming and relatively quiet. In recent years however, there has been a burst of large and moderate earthquake activity in east-central Iran. Some of the more significant ones include the (i) June 10, 1939 ($m_b = 5.5$) Baharestan earthquake (ii) August 31, 1968 ($M_S = 7.3$) Dasht-e-Bayaz earthquake, (iii) September 1, 1968 ($M_0 = 3.0 \times 10^{20}$) Ferdows earthquake, (iv) May 5, 1973 ($m_b = 5.1$) Shahzadeh earthquake (v) June 17, 1974 ($m_b = 4.8$) Posha earthquake (vi) November 27, 1979 ($M_S = 7.1$) Qainat earthquake, (vii) December 26, 2003 ($M_w = 6.6$,

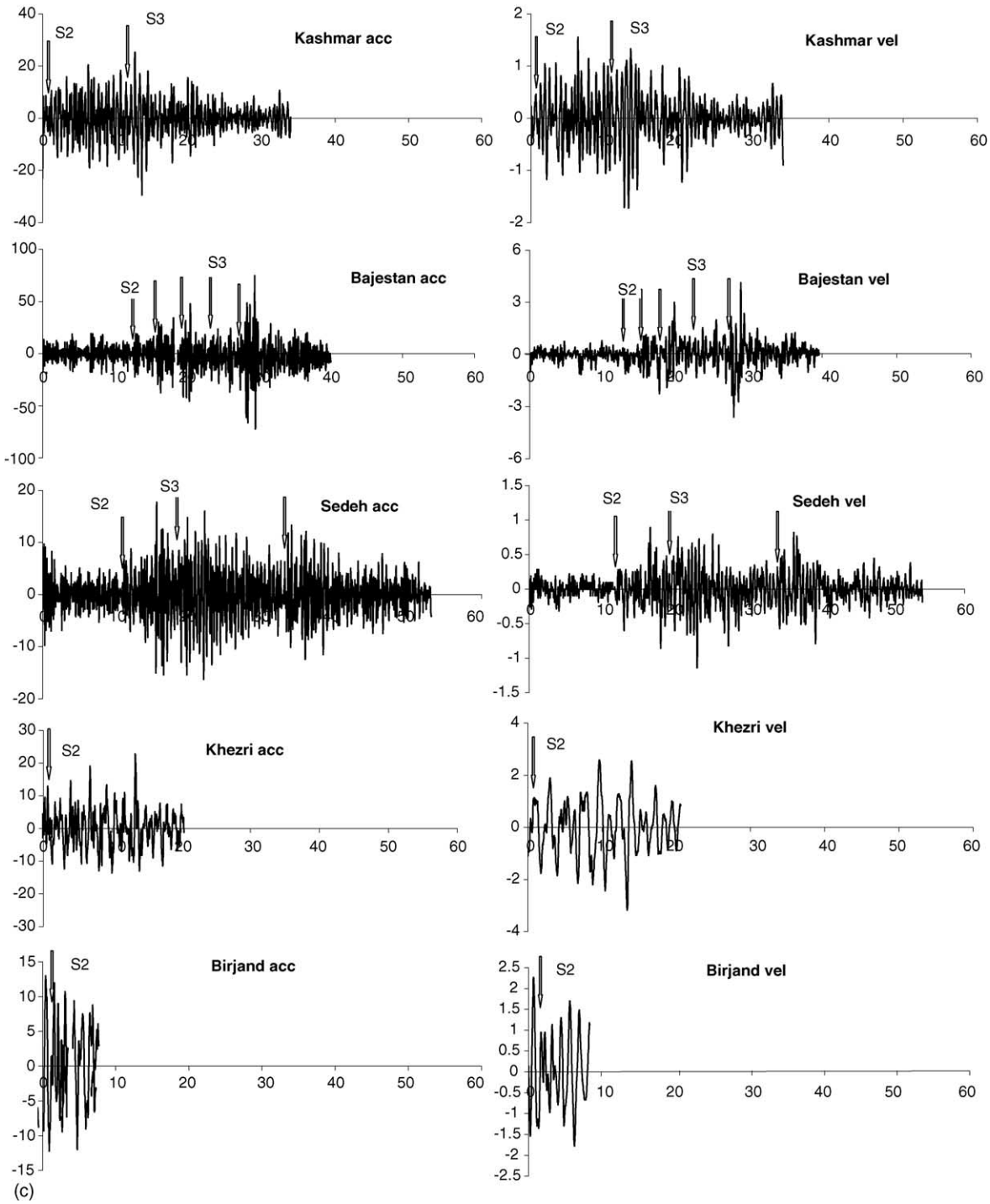

Fig. 1. (*Continued*).

$M_0 = 0.92 \times 10^{19}$) Bam earthquake and (viii) the September 16, 1978 ($M_S = 7.7$) Tabas earthquake, that we investigate in this study here (Fig. 1a).

Tabas earthquake is associated with a concealed Quaternary thrust fault located at the base of a series of low hills, made up of Neogene clay deposits, separating the Shotori fold-thrust mountain belt (to the east) from the Tabas playa (to the west) (Fig. 1a). Major strike slip faults, ending in thrust faults whose displacement die away towards the ends, are widespread within east-central Iran. Such faults are a manifest of the style of shear deformation caused in the east Iranian block by the active convergence process of the Arabian and Eurasian plates and the Tabas earthquake is considered to have occurred on a listric thrust fault system (Berbarian, 1982; Walker et al., 2003).

Various estimates of the Tabas hypocentral locations, based on regional (Atomic Energy Organization of Iran (AEOI); Bulletin of the Seismographic Network of Mashad University (BSNMU)) and teleseismic (National Earthquake Information Center (NEIC); International Seismological Centre (ISC); Harvard Centroid Moment Tensor (CMT) solution; Moscow Institute of Physics of the Earth(MOS); Centre of Seismologique, Euro-Mediterranean (CSEM); Berbarian, 1982 and Engdahl et al., 1998) recordings, are available. Of these, the location by Engdahl et al. (1998), that is obtained on the basis of arrival times of PKiKP, PKPdf, depth phases pP, pwP, sP in addition to regional and teleseismic P and S phases, is considered by us to be better constrained. The location errors for the estimated hypocenters may be as large as 10–15 km (Berbarian, 1979a). However, it is noteworthy that the estimated epicenters all lie within 20 km from each other, at the southeastern end of a geologically identified prominent surface break, believed to have been involved in the Tabas rupture process (Berbarian, 1982).

The strike, dip and rake of the causative fault, estimated by different investigators from far-field data, are also varied. While the estimated strike, dip and slip of (i) Berbarian et al., (1979) viz. 332°N, 31° and 107°, respectively, from long period P-wave first motion data (ii) Niazi and Kanamori (1981) viz. 330°N, 30°, 110°, respectively, from moment tensor inversion of R_1 and R_2 phases from the IDA network and (iii) CMT solution viz. 328°N, 33°, 107°, respectively, are comparable, i.e. here the fault planes are striking in approximately WNW–ESE direction and having moderately high dips, (iv) the results of inversion of P and SH-waveforms available from far-field WWSSN network data viz. 355°N, 16° and 155° (Walker et al., 2003) are somewhat different viz. here the fault plane is striking in nearly N–S direction and having low dip. The former interpretation of the fault plane (strike of WNW–ESE) is more in line with the regional strike of the exposed faults in the region.

Several investigations suggest that the Tabas earthquake had a complex faulting process. For example, (i) a prominent, generally NNW–SSE trending surface rupture, following the low anticlinal hills of the Tabas fold system lying to the west of the Shotori ranges, possibly associated with the co-seismic phase of the earthquake process, was identified from a detailed geological investigation (Berbarian, 1979b). This rupture, about 85 km in length, was splayed into 8–10 discontinuous and randomly distributed segments that extended over a zone of about 30 km width. (ii) Berbarian (1982) analyzed local recordings of one of the major aftershock sequences and opined that faulting had initiated at a depth greater than 8 km, at the southern end of the causative fault, near the basement, below the frontal sections of the Shotori fold-thrust belt and then propagated upwards, in a northwesterly direction along listric thrust planes to intersect the earth surface as a major rupture. As the propagating fault approached the surface, it splayed into several fault segments and ruptured the surface. (iii) Walker et al. (2003) viewed such a pattern of surface deformation as evidence of the occurrence of discrete earthquake events. These authors identified on digital topography and ASTER satellite imagery several indications of long-term and co-seismic growth within the Tabas fold system. From these they suggested that (a) such a fold growth had accommodated the major part of the complex fault thrust movement at depth and (b) the process of co-seismic rupture and long-term folding caused these apparently discontinuous, surface rupture segments. (iv) Shoja-Taheri and Anderson (1988) identified four sub-events on strong motion records of the Tabas earthquake which they inferred had occurred on the fault as the rupture propagated unilaterally in a northwesterly direction. (v) Hartzell and Mendoza (1991) analyzed strong motion records from three selected stations (Tabas, Bosroyeh and Deyhook) and also some selected WWSSN teleseismic P-waveforms. They found that the WWSSN stations located to the southeast of the earthquake

recorded multiple arrivals; but on records of stations located at other azimuths, these arrivals coalesced and could not be resolved well. Further they opined that the strong motion data exhibited signatures of directivity to the northwest. Hartzell and Mendoza (1991) used a least square technique to simultaneously invert this near and far field data. Their numerical analysis indicated that rupture (a) occurred due to unilateral rupturing to the northwest, (b) as a multiple source event, with four main source regions over a fault length of 90 km.

We may remark here that, as in other parts of the world, where large earthquakes with complicated patterns of energy release have been found to be multiple events (e.g. Wyss and Brune, 1967; Kanamori and Stewart, 1978), several large magnitude earthquakes occurring within the complex tectonics of the Iranian plateau are also in actuality multiple events (see for example Campos et al., 1994; Sarkar et al., 2003).

In this study we investigate the near field accelerograms from the Tabas earthquake recorded by a strong motion array installed in east-central Iran by Building and Housing Research Center, Iran. Our aim is to infer about the characteristics of the source and its rupture history as seen on near field 'SH-wave' accelerograms. We try to correlate the bursts of energy signatures on these accelerograms in term of sub-events of the Tabas earthquake and infer about their fault plane solutions, seismic moment, asperity size, seismic energy release and provide some insight into the scaling relations for these estimated parameters. We also estimate from accelerograms the average shear wave quality factors at the recording sites. We have employed near field 'SH-waves' in our investigation because these are minimally affected by the crustal heterogeneities (Haskell, 1960) and do not require any correction for mode conversion at the free earth surface. So we could adopt a half space representation for the earthquake source region during the 'SH-wave' data analysis. We note here that the approach followed here in this study, albeit very simplistic, has already been successfully applied in the analysis of two other earthquakes viz. the large ($m_b = 6.4$, $M_S = 7.7$, $M_w = 7.3$) June 20, 1990 Rudbar earthquake of Iran (Sarkar et al., 2003) and the moderate ($m_b = 6.5$, $M_S = 7.0$, $M_w = 6.8$) October 19, 1991, Uttarkashi earthquake of India (Kumar et al., 2005).

For our investigation, we first rotate the observed horizontal component accelerograms appropriately to derive transverse component accelerograms. We assume here that these approximately represent SH-wave accelerograms. We next identify the strong high frequency bursts of energy on these 'SH-wave' accelerograms, as well as the corresponding impulsive strong phases on the counterpart velocity seismograms, as signatures of discrete sub-events. The sub-events are located using the ensemble of relative times from various recording sites with respect to a sub-event, whose location is assumed to be known (to be explained below). Our basis here is that a particular burst recorded at a station represents a new source of energy radiation from the related asperity (sub-fault) on the fault. We consider each strong phase available from those particular accelerograph stations that recorded it distinctly and assemble the set of such phase recordings for each of the sub-events. Next we estimate the corresponding 'SH-wave' spectra, which is compensated for geometric divergence. On the ensemble of spectra of each sub-event, we conduct a non-linear least square inversion to obtain an average estimate of the strike, dip and slip of the corresponding rupture (Sarkar et al., 2003). The analysis is confined to the high fidelity band of the observed spectra. After suitably compensating the observed spectra for geometric divergence, inelastic attenuation and free surface effect, we fit appropriate Brune ω^{-2} models to the displacement spectra in the high fidelity range of frequencies. The best fit Brune models allow to extrapolate the empirical spectra to frequencies outside the recorded bandwidth and estimate appropriate values for (i) corner frequency and (ii) zero frequency spectral level and thereby the seismic moment, moment magnitude, asperity size, stress drop and shear wave energy released by the asperity. In this manner we have been able to estimate/infer (i) the locations of four/five asperities (sub-faults) associated with distinct phases of energy release, (ii) their relative time of occurrence and (iii) the corresponding source parameters. We could use this corpus of information to identify the localized imprints of the earthquake slip process and gain some insight into the details of the complex rupture process.

2. Data set

The strong motion array consists of 20 accelerograph stations installed within a radius of 300 km from Tabas. All the instruments are of SMA-1 type with a threshold of 10 gal. Although the array was fully oper-

Table 1
Details of the accelerograph stations

Station	Station coordinates			Component orientation	Hypocentral distance (km)	PGA (g)	Duration of operation (s)
	°N	°E	km				
Bajestan	34.52	58.18	1.24	N59°E (L)	160.86	0.08	39.58
				N31°W (T)		0.06	39.60
				Up (V)		0.02	39.60
Birjand	32.88	59.21	1.46	S24°W (L)	180.72	0.01	8.42
				S66°E (T)		0.01	8.42
				Up (V)		0.01	8.42
Boshroyeh	33.86	57.42	0.88	N79°E (L)	68.53	0.11	51.09
				N11°W (T)		0.09	51.09
				Up (V)		0.08	51.09
Deyhook	33.29	57.50	1.36	N80°W (L)	16.12	0.30	58.38
				S10°W (T)		0.38	58.38
				Up (V)		0.16	58.38
Ferdows	34.01	58.16	1.24	S20°E (L)	113.26	0.07	53.02
				N70°E (T)		0.10	52.96
				Up (V)		0.05	52.96
Kashmar	35.23	58.46	1.04	S74°E (L)	243.21	0.01	33.90
				N16°E (T)		0.02	33.92
				Up (V)		0.01	33.90
Khezri	34.02	58.81	1.55	N61°W (L)	162.06	0.02	20.60
				S29°W (T)		0.02	20.58
				Up (V)		0.02	20.60
Sedeh	33.33	59.23	1.65	S24°W (L)	178.14	0.01	54.18
				S66°E (T)		0.01	54.20
				Up (V)		0.01	54.22
Tabas	33.60	56.93	0.69	S74°W (L)	58.90	0.88	48.99
				S16°E (T)		0.93	48.99
				Up (V)		0.75	48.99

ational at the time of occurrence, the earthquake triggered only nine accelerographs. Table 1 lists the salient features of these nine stations while their geographical locations are shown in Fig. 1a.

We note that the accelerographs are sparsely distributed in relation to the overall size of the fault and do not have a good spatial coverage. Local strong motion records are generally known to be more sensitive to faulting of those sections of the fault closest to the station, while the more distant stations are unable to contribute suitable constraints for these sections of the fault (Mendoza and Hartzell, 1989). We also note that (i) the accelerogram data does not have a common time code and (ii) the filter characteristics used in recording are not available with us. These deficiencies have somewhat constricted our procedure of analysis and inference.

We assume that the Tabas earthquake rupture initiated from the hypocentral location given by Engdahl et al. (1998). Using the back azimuths (θ) from the nine accelerograph stations to this epicenter, we suitably rotate the radial (L) and transverse (T) components of the recorded acceleration to obtain accelerograms parallel and transverse to the azimuth directions. The derived transverse accelerograms (Fig. 1b) exhibit several high frequency bursts of energy that we interpret to be representing energy radiation from discrete asperities on the main causative fault. For if such high frequency energy signals were to be the result of near surface resonance effects, these should be seen all along the accelero-

grams and not just as localized packets in time in the accelerograms.

We have been able to identify on the acceleration and corresponding velocity records (see Fig. 1b) five to six distinct phases of energy bursts (marked as S1, S2, S3, S4, S5, S6) which are co-relatable spatially. These phases have been identified on the basis of their impulsive beginnings that are followed by a substantial energy packet on the velocity records and high frequency energy packets on the acceleration records. We may note here that Fig. 1b is actually a better representation of the 'SH waveforms' for the main burst of

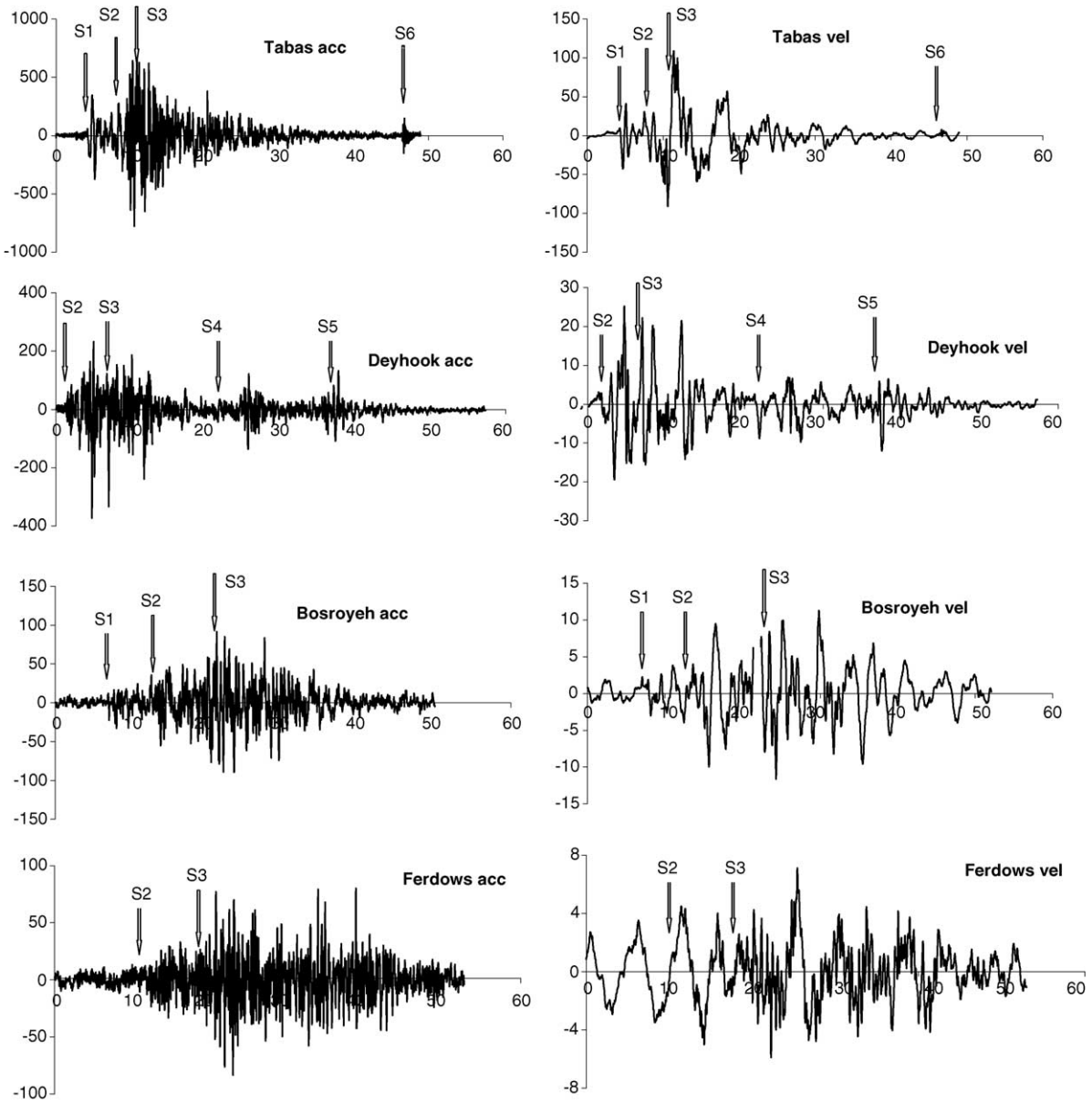

Fig. 2. The transverse accelerograms ('SH-wave' accelerograms') for the S3 phase of energy, derived from rotating the horizontal accelerograms through the back azimuth angles from the S3 epicenter to the seven stations (see text) and the corresponding velocity seismograms are shown. Note that, compared to (b) the signatures of S3, S4, S5 and S6 phases of energy release are clearer in this figure.

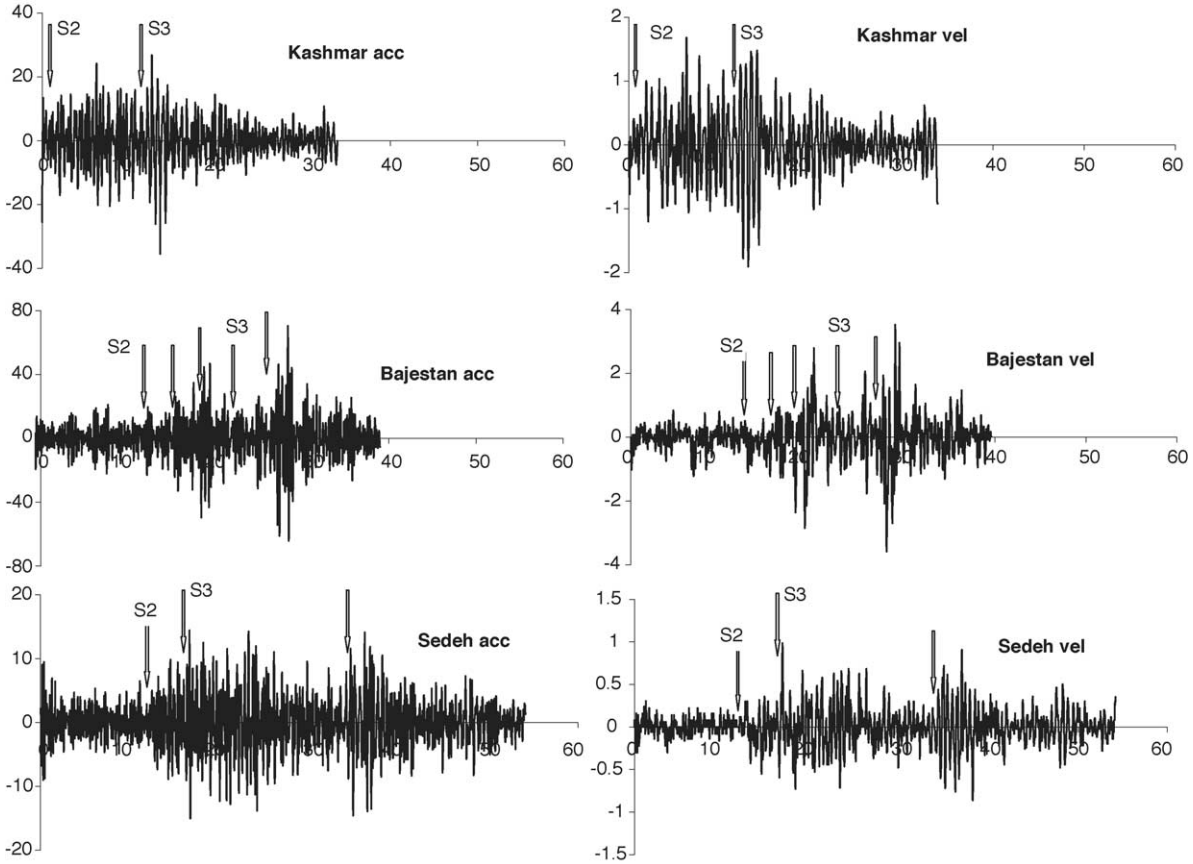

Fig. 2. (*Continued*).

energy (identified as S2 phase in the figure) as we have used the sub-event location of S2 for rotation of accelerograms. For the other five bursts of energy phases (S1, S3, S4, S5, S6), as this rotation is not optimal, their representation as transverse components can be improved further by using appropriate locations of the sub-events. In Fig. 2 we show the transverse accelerograms that were obtained after rotating the horizontal accelerograms through the back azimuth angles from the S3 sub-event (which we have determined later in this study) to the seven stations recording it. We also show here, in this figure, the corresponding velocity seismograms. These, we find, are a better representation of the 'SH waveforms' for the S3 burst of energy.

A few bursts of energy are occurring on Bajestan and Sedeh records for which we were unable to find co-relatable phases in the records from the other sites. For the present they remain unexplained in terms of sub-event sources. They are likely to represent weak shocks occurring in the immediate vicinity of the above recording stations and are thus not recorded as strong phases in the other stations. It is known that a considerable number of aftershocks were recorded in the general area around the main earthquake and it is possible that a few small spatially scattered events may have occurred nearly simultaneously with the main shock.

3. The characteristics of the observed 'SH-wave' accelerograms

The sparsely distributed nine accelerograph stations can be broadly grouped into two categories depending on their locations with respect to the surface ruptures.

While Tabas lies closest to the northern end of the NNW–SSE trending ruptures, on the northwestern side, all the other eight stations are located on the northeast/southeastern side of these ruptures at varying distances from these. Amongst this second set of eight stations, Deyhook, located closest to the epicenter of the main sub-event, from where the rupture process presumably initiated, is at the southeastern end of the rupture. The other seven stations are scattered at larger distances. Boshroyeh and Ferdows are aligned along a line almost perpendicular to the general strike of the surface ruptures and situated 70 km and 113 km, respectively away from these. The other five stations (Khezri, Bajestan, Sedeh, Birjand and Kashmar) are farther away from the main sub-event epicenter as also from the traces of the surface ruptures. Khezri, Bajestan, Sedeh and Birjand are about 160–170 km away, while Kashmar, the farthest, is more than 240 km away. Also Tabas and Boshroyeh, situated on either side of these northwest–southeast oriented surface ruptures, are at approximately equal distance from the main sub-event epicenter.

As mentioned earlier, a number of investigations have concluded that the rupture initiated from the southeastern end of the fault and proceeded unilaterally in a northwestern direction. The signatures of such a mode of rupture propagation can be seen clearly in the 'SH-wave' accelerograms (see Fig. 1a and b) from Deyhook, Tabas, Boshroyeh, Ferdows and Bajestan. Since Deyhook is located at the southeastern end of the fault system, exactly opposite to the (northwest) direction of rupture propagation, the signature of 'SH-wave' energy release on the observed accelerogram here is spread out. On the other hand, since Tabas is located at the northern end of the fault system and directly in the direction of the northwesterly propagating rupture, due to Doppler effect, the 'SH-wave' accelerogram exhibits front loaded energy release. Further since this station is situated closest to the region where this propagating rupture terminated, less than 3 km from the fault outcrop (Shoja-Taheri and Anderson, 1988), the seismic energy observed here is largest and is more than at Deyhook, which although located closer to the source of main energy release, lies opposite to the direction of rupture propagation. Of course, the effects of the local site conditions have also played their amplification role here. For, while Deyhook is located within thin sediments that occur in the flank of the limestone hills, Tabas lies within thick, low velocity alluvial deposits. Shoja-Taheri and Anderson (1988) opine that the large amplification of seismic wave energy at Tabas could also be due to the velocity of rupture propagation being smaller than the shear wave velocity in the basement but greater than that in the overlying sediments.

Boshroyeh, Ferdows, and Bajestan are centrally placed, on the broader sides of the surface trace of the rupture, but not in the immediate direction of the unilateral rupture propagation. So the accelerograms from these stations show, again due to Doppler effect, a gradual build up and tapering of energy, in the form of a cigar. At distant Sedeh, located on nearly the same latitude as Deyhook but several kilometers away from it and from the main sub-event epicenter, the energy build up is somewhat sharp but of very low amplitude. At Kashmar this building up effect is indistinct and on a low scale, due to its large epicentral distance and also possibly because triggering occurred here at a later stage of the earthquake process (Shoja-Taheri and Anderson, 1988). At Tabas, Deyhook, Boshroyeh, Ferdows and Bajestan, the earlier arriving energy is from the P wave related phases of relatively small amplitude. These are followed by strong S phases that come from the breaking asperities and then finally there is coda energy in the tail part of the accelerogram. This feature is not so clear at Sedeh, Kashmar, Khezri and Birjand due to the large hypocentral distance as well as instrumental problems for the last two mentioned stations.

From an overall view of these 'SH-wave' accelerograms and velocity seismograms, we note that two subevents (S2 and S3 phases) with major energy releases are well identifiable on Tabas, Deyhook, Boshroyeh, Ferdows, Bajestan, Sedeh, and Kashmar. However, at Khezri and Birjand, due to weak signal-to-noise ratio, a very small segment of waves are recorded and various phases are not seen. We suggest that the acceleration and velocity records from these two latter stations represent the release of the S2 phase, which triggered their recording. Notably, the time separation of the arrivals of S2 and S3 phases at Deyhook and Tabas is almost equal, about 6 s. Also the ratios of their peak amplitudes (i.e. AS2(D)/AS3(T), etc.) are nearly equal. At the other five stations, while the time difference of these two phases is always larger, the ratio of their peak amplitudes is smaller. On the basis of these observations we conclude that S3 epicenter is most likely located

within the surface rupture zone, at a point on the rupture zone that is equidistant from Deyhook and Tabas.

The accelerograms and velocity seismograms at Tabas and Boshroyeh also record another significant phase of energy release S1, approximately 5 s before the S2 phase. This phase is about one-third as strong as S2 phase but has nearly the same frequency content. At Deyhook, the signature of S1 is weak and not clearly identifiable, perhaps a manifestation of localized path effects. At Ferdows and the other more distant stations, the phase cannot be identified at all. Therefore we interpret that this weak sub-event occurred closer to Tabas, Deyhook and Boshroyeh.

Two more sub-events (S4 and S5 phases) seen on the Deyhook accelerogram/velocity seismogram alone and one sub-event (S6 phase), seen on the Tabas accelerogram/velocity seismogram alone, are of comparable amplitude and frequency content. These two phases appear to have occurred about 20–30 s after S3. Due to the absence of a common time code, it is somewhat difficult to directly correlate S6 with either S4 or S5. However, we note that S4, S5 and S6 have nearly equal peak amplitudes and are of approximately the same frequency content. Also these phases are not seen on Boshroyeh or the other stations. These observations suggest that the above three sub-events are small and occurred within the Tabas depression region, between Tabas and Deyhook, where the fragmented surface ruptures lie randomly, in a complicated manner (see Fig. 1a). In a later section (see Section 5), we provide some indirect evidences that seem to intimate that S5 and S6 possibly represent the same sub-event.

4. Analysis of data

4.1. Location of the sub-events

The derived 'SH-wave' accelerograms and the corresponding velocity seismograms are shown in Fig. 1b. The picks, marked as S1, S2, S3, S4, S5 and S6, show the positions of the six different sub-event arrivals. It is recognized that the precise reading of arrival times of phases, particularly the S-wave phases become a challenging task on account of earlier arriving energy. It is much more so while using accelerograms for the purpose. We have employed two characteristics of the waveforms towards this end. Firstly, on the accelerograms, we found distinct arrivals of very high frequency energy packets arriving at discrete intervals. This we have interpreted as the radiation from the breaking asperities or sub-faults in the complex rupture process. We note that such packets of high frequency energy could not be the result of near surface site effects as, in that case, such high frequencies should be present all along the accelerograms and not just in packets as has been observed. Secondly, in the corresponding velocity waveforms we use the conventional approach to pick the arrivals of 'SH-waves' by taking note of impulsive beginnings of high amplitude phases. We could find very good correspondence of the picks from the acceleration and velocity waveforms, in all cases within ± 0.2 s at the most.

In the absence of a common time code, it was not feasible to locate independently the hypocentres of these sub-events on the basis of the accelerogram/velocity seismogram data. However, we employed a master event technique to provide an estimate of the hypocentral location of the sub-event from where the S3 phase of energy was possibly radiated. In this scheme we (i) chose the S2 sub-event as the master event and (ii) assumed that it was located at the hypocentre estimated by Engdahl et al. (1998). We next noted the shear wave arrival times from the S3 sub-event relative to the shear wave arrival times from the S2 sub-event at the seven stations Tabas, Deyhook, Boshroyeh, Ferdows, Sedeh, Kashmar and Bajestan. It is noteworthy that these seven sets of relative arrival time readings that we separately estimated from the acceleration and velocity data were very well comparable and differed at most by an order of 0.18 s (at Ferdows). We now numerically inverted these (seven) relative shear wave arrival time readings, using a master event technique (Sarkar et al., 1995; Hamzehloo et al., 1997; Sarkar et al., 2003) and estimated that the S3 phase of energy was released from 33.29°N, 57.12°E, at 8.2 km depth, 9.0 s after the release of the S2 phase of energy (see Fig. 1a). The standard error of location of the S3 hypocentre is estimated to be 5.2 km. We note here that because of the poor azimuthal coverage of the stations and the large distance (more than 115 km) of four of these (viz. Ferdows, Sedeh, Kashmar and Bajestan) from S2, the estimates of the focal depth and relative time of occurrence of S3 are considered to be not quite as reliable as its epicenter.

The sub-event corresponding to the release of S1 phase of energy is well recorded on Tabas and

Boshroyeh records only. We note that the difference in shear wave arrival times from S1 and S2 at Tabas is smaller (nearly 2.5 s) than at Boshroyeh implying that S1 epicentre is closer to Tabas than Boshroyeh. However, this limited data is not enough to numerically estimate the parameters of epicentral location and the time of occurrence of S1 as such by using a master event technique as above. But (i) assuming that the Tabas accelerograph was triggered by the P-wave from the S1 sub-event and then considering (ii) the estimated (S–P) times from Tabas station and (iii) the times of shear wave arrival from the S1 sub-event relative to that from the S2 subevent at Tabas and Boshroyeh we may suggest that the S1 phase of energy was probably released approximately from the location 33.6°N, 57.2°E, about 5.7 s prior to the main (S2) phase of energy release. This position lies within the zone of high angle reverse faults that lie to the immediate east of Tabas (see Fig. 1a).

In Fig. 2, we show the SH-wave accelerograms that were obtained by suitably rotating the horizontal accelerograms using the back azimuth (θ) to the S3 epicenter (estimated above) from the seven stations Tabas, Deyhook, Boshroyeh, Ferdows, Sedeh, Kashmar and Bajestan. We also show in this figure the corresponding velocity seismograms. A noteworthy point in this figure is that here the signatures of the phases S4, S5 on Deyhook accelerogram and S6 on Tabas accelerogram are now more accentuated and clear than were these in Fig. 1b. This indicates that the angle of rotation we employed for S3 is more appropriate for these three sub-events as well. On the basis of this observation we conjecture that the locations of the epicenters, from where the S4, S5 and S6 phases of energy were released, lie on the same major rupture on which the epicenter of the S3 phase of energy is located (see Fig. 1a).

4.2. Source parameters of the sub-events

We next computed the acceleration spectra for each of the six phases of energy. Our expectation was that these would give information about the sub-faults or asperities that provided dominant contributions to the ground motion at the various sites during the release of these phases of energy. These may include the direction of rupture and orientation and size of the related asperity.

The acceleration spectra were obtained using relevant time windows on the appropriately rotated transverse component accelerograms. We used Fast Fourier Transform (FFT) along with a Hamming-Tukey window to reduce the effect of data reduction. Several variations on the window sizes and placement were performed to confirm the stability of these spectra in terms of their general structure and frequency content. We discuss below about some important characteristics of the spectra for S2, S3 and S1, exhibited in Figs. 3–5, respectively.

We note in Fig. 3 that the flat portion of the acceleration spectra of S2 sub-event (corresponding to the ω^{-2} Brune source model) generally lies between the frequencies 0.2 and 6 Hz or so. Also that at the lower frequency end, where a slope of +2 is expected, corresponding to the flat portion in the corresponding displacement spectrum (see Fig. 6), the drop of energy appears to occur at around 0.2–0.4 Hz. This frequency appears to be too high to be the corner frequency (f_c) for the S2 sub-event because then, with an assumed uniform SH-wave speed 2.0 km/s, this would imply an asperity of area about 12–15 km^2 and a seismic moment of the order of 0.5×10^{17} N m only. In Fig. 4 (and Fig. 6) also, for the case of S3 phase of energy release, we note a similar fall off in energy at about the same frequency. In Fig. 5, the spectra of S1 sub-event, at Tabas and Boshroyeh, appear to be corrupted because of the weak signal of the event. Here also the apparent corner frequency appears to be too high, around 0.4 Hz. We further note that although these three sub-events are expected to have substantially different magnitudes, their corner frequencies are nearly the same. All this leads us to suspect that a low cut filter with a cutoff frequency around 0.2 Hz or so has been used so that the long period energy have been kept out of the accelerograms.

In all these spectra (Figs. 3–5), the energy drop-off at the higher frequency side is the Hanks frequency (f_{max}). We note that for S2 (Fig. 3), while f_{max} is about 7 Hz, the dominant trend of exponential decay is actually initiated near 3–5 Hz or so. This frequency, denoted as f_E by Anderson and Gough (1984), is larger than the corner frequency (f_c) and could be seen more clearly on semi-log plots of the acceleration spectra. For the sake of brevity, we have not shown the semi-log plots here.

We also see that, compared to the three nearest stations viz. Deyhook, Tabas and Boshroyeh, the high

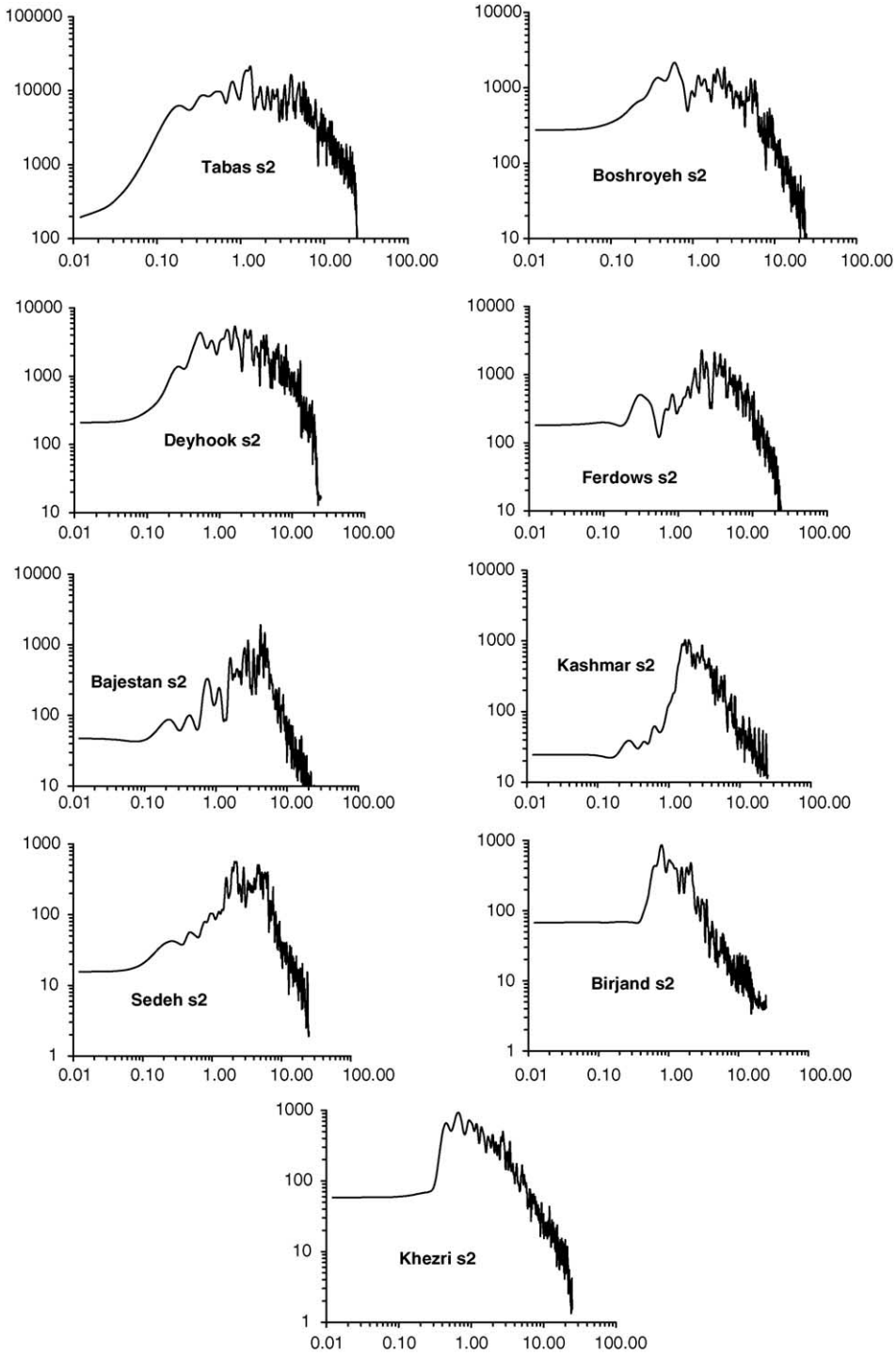

Fig. 3. The observed acceleration spectra for the main sub-event S2 (see text) from the nine stations recording it. The horizontal axis denotes frequency in hertz; the vertical axis denotes spectral amplitude in cm/s.

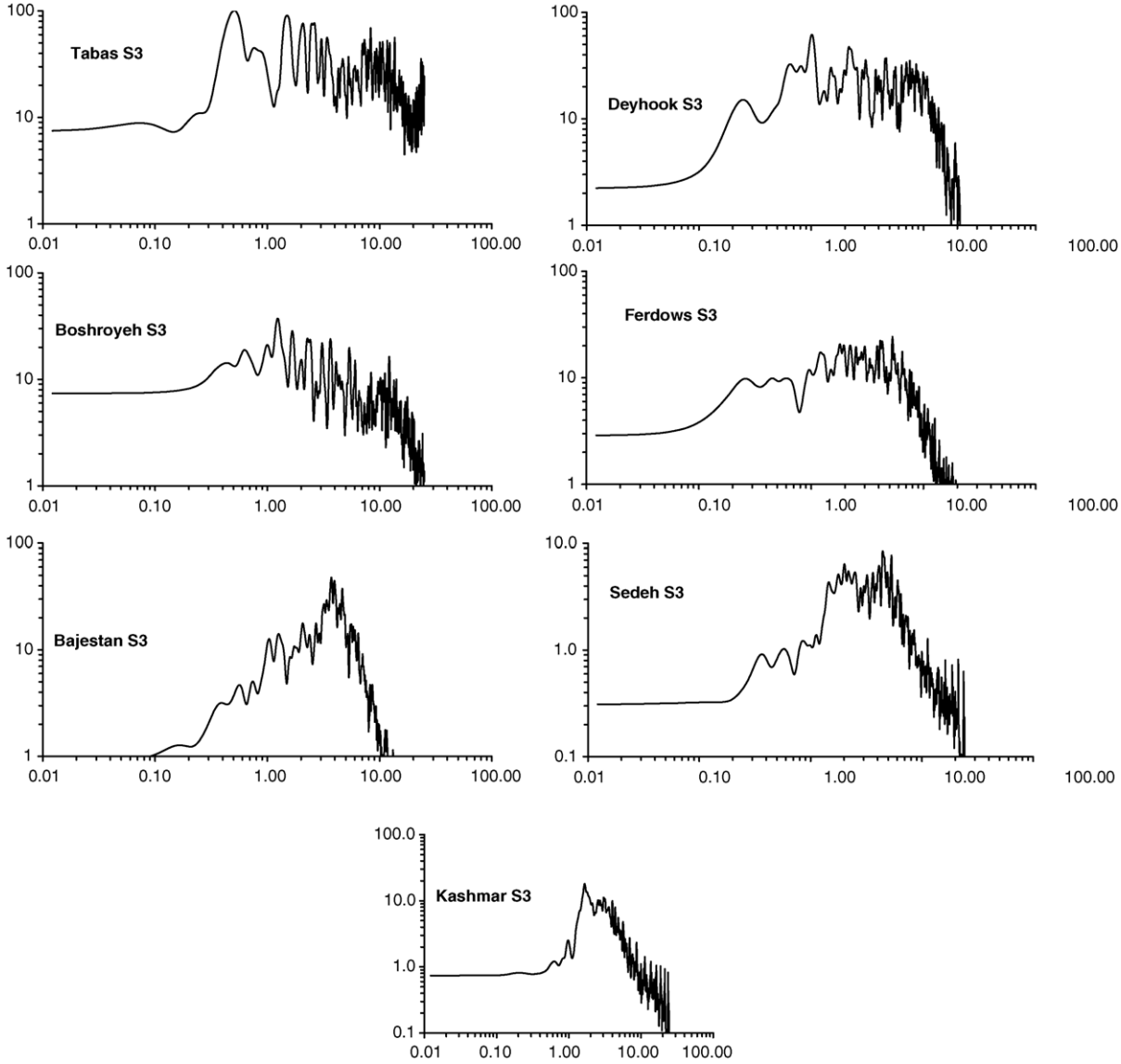

Fig. 4. The observed acceleration spectra for the sub-event S3 (see text) from the seven stations recording it. The horizontal axis denotes frequency in hertz; the vertical axis denotes spectral amplitude in cm/s.

frequency spectral energy falls off more rapidly at the more distant stations viz. Ferdows, Bajestan, Sedeh, Birjand and Khezri. A similar pattern of high frequency fall off, beginning at about 3–5 Hz (f_E), is also observed for the sub event S3 (Fig. 4). Here also f_{max} is about 7 Hz or so. For the sub event S1 (Fig. 5), while f_{max} has the same value (viz. 7 Hz), f_E appears to be higher, having a value of approximately 5–6 Hz. We also note in Figs. 3 and 4 that at Boshroyeh, Ferdows, Bajestan and also to some extent at Sedeh and Kashmar, there are sharp spectral peaks and holes, indicative of low velocity near surface sedimentary structure. Indeed, geologic investigations show that Ferdows, Bajestan and the surrounding region lie on an alluvial plain within heavily deformed Jurassic sediments and Quaternary alluvial deposits shed from rivers flowing from

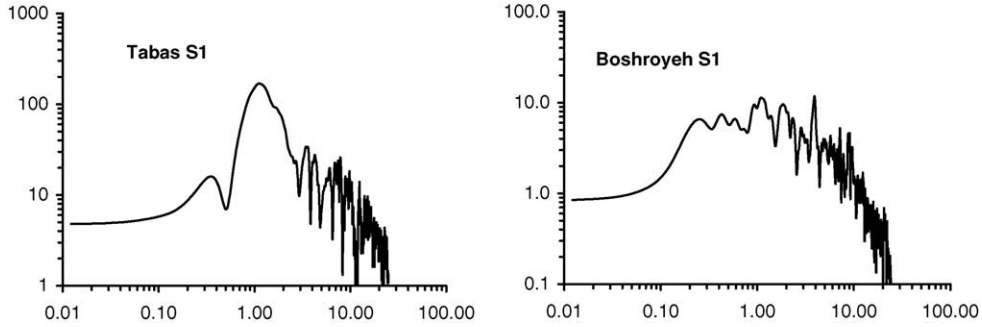

Fig. 5. The observed acceleration spectra for the foreshock S1 (see text) from the two stations recording it. The horizontal axis denotes frequency in hertz; the vertical axis denotes spectral amplitude in cm/s.

the neighbouring Kuh-e-Kalat mountain range lying to the east. LANDSAT TM images of the region also show the presence of prominent river incision and uplift of these alluvium deposits and river terraces formed within the clay and salt flats (Walker et al., 2003).

Since the processed accelerograms available for the present study are low cut filtered, we are unable to use these directly for an appropriate estimation of the corner frequencies and also the corresponding long period spectral amplitudes that are necessary for calculating the source parameters of any of the identified sub-events. To circumvent this problem, we consider the following.

Since the fault plane solution is preserved in the entire spectrum, any section of it can be used for estimating the strike, dip and slip of the fault plane for at least some of the sub-events. With this consideration, for the sub-events S1, S2 and S3, we pick the observed spectral 'SH-wave' amplitudes of the acceleration at a common frequency (f, say) on all possible stations, convert these into the corresponding spectral displacements and correct these values for geometric divergence. The corresponding theoretical estimates can be obtained from the formula for radiation pattern for far field SH-waves from a point double couple source (see, for example, Aki and Richards, 1980, equation 4.86; Lay and Wallace, 1995, equation 8.65). This formula depends on the fault orientation parameters (i.e. fault strike, dip and slip), source take off angle and station azimuth. We now define an error function E(fault strike, dip, slip) as

$$E(\text{fault strike, dip, slip}) = \sum_i (A_{oi} - A_{ti})^2 \qquad (1)$$

where A_{oi} and A_{ti} denote the observed and theoretical estimates of the spectral amplitude of displacement at the ith station of the ensemble of stations and optimize this function in the least square sense to simultaneously obtain suitable estimates for the strike, dip and slip of the causative fault of the particular sub-event. Thus assuming a double couple source model and using the corrected observed spectral amplitude of displacement data from (i) nine stations, for the S2 sub-event (Fig. 3) and (ii) seven stations, for the S3 sub-event (Fig. 4), and employing the non-linear Newton technique for optimization purpose (Sarkar et al., 2003) we could thus provide estimates of the strike, dip and slip on the two nodal planes of the fault plane solution of these two sub-events.

The estimated fault plane solution corresponding to the S2 sub-event is as follows: NP1: strike = 357.3°N, dip = 15.7°, slip = 155.9°; NP2: strike = 110.0°N, dip = 83.0°, slip = 75.0°. Considering the regional tectonics, our preference is for the ESE–WNW striking, steeply dipping nodal plane with approximately reverse thrust motion as the fault plane of S2, as the strike of this plane is sub-parallel to the regional strike of mapped faults. The standard error of estimate of NP2 is 0.60. As mentioned earlier, this event is assumed to have occurred at 33.25°N, 57.38°E, at 9.0 km depth.

For the causative sub-fault corresponding to the S3 sub-event, the following estimates are obtained: NP1: strike = 355.0°N, dip = 16.1°, slip = 156.8°; NP2: strike = 107.0°N, dip = 83.0°, slip = 75.0°. Here also, for the reasoning given above, our preference is for the ESE–WNW striking, steeply dipping nodal plane with approximately reverse thrust motion as the fault plane

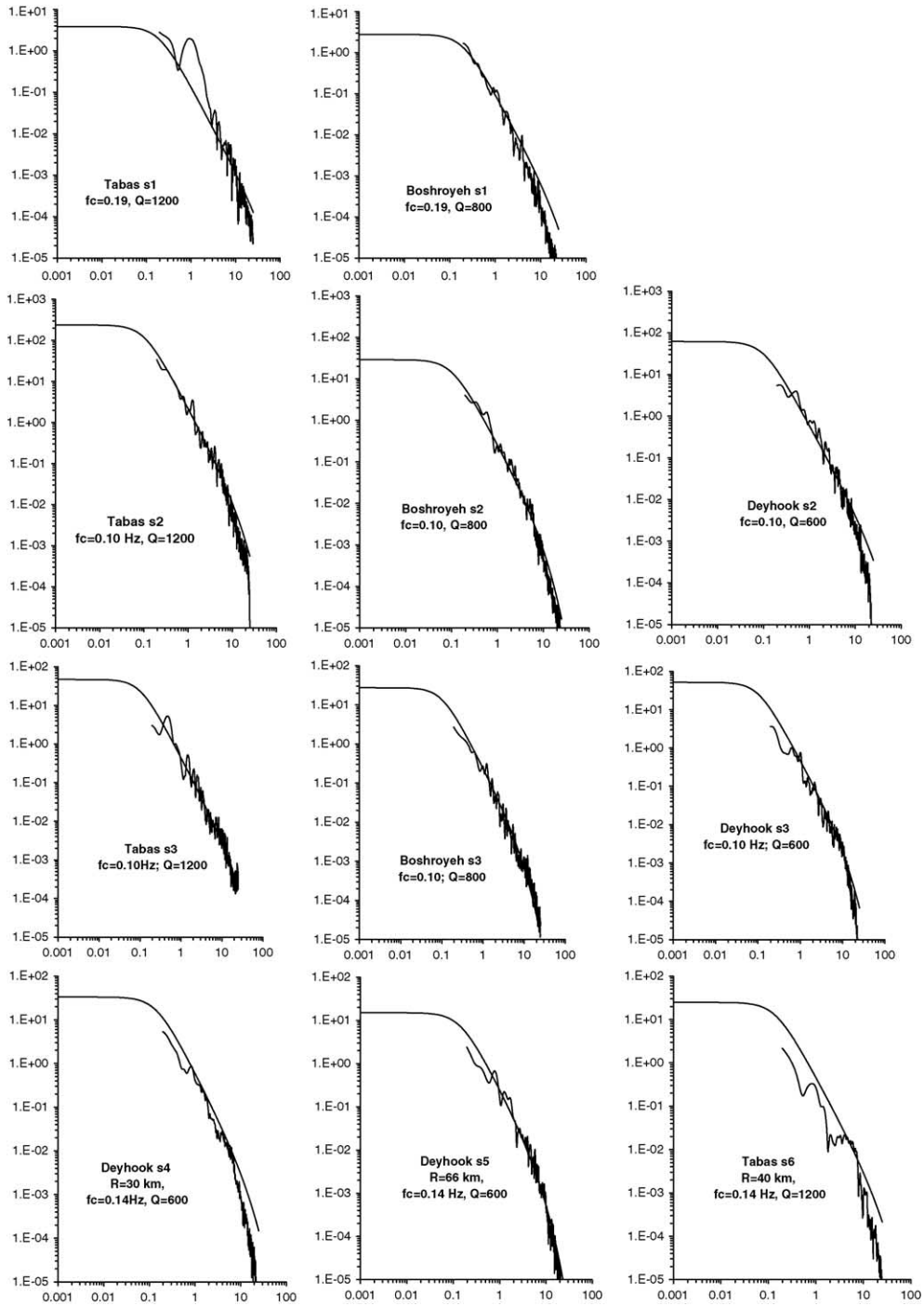

Fig. 6. The observed 'SH-wave' displacement spectra along with the corresponding best fit Brune spectrum for the sub events S1, S2, S3, S4, S5 and S6 at the three closer stations viz. Deyhook, Tabas and Boshroyeh. The horizontal axis denotes frequency in Hz; the vertical axis denotes the amplitude spectral density in cm s.

of S3. The standard error of estimate of NP2 is 1.16. We have earlier estimated that the hypocentre of S3 is located at 33.29°N, 57.12°E, at 8.2 km depth and that this sub-event occurred 9.0 s later than the sub-event S2.

The two station spectral data from Tabas and Boshroyeh pertaining to S1 (Fig. 5) is inadequate to directly use the non-linear Newton scheme for optimizing E(fault strike, dip, slip) in the least square sense for estimating the strike, dip and slip of this causative sub-fault. So here we used a grid search technique and estimated that the sub-fault that radiated S1 phase of energy has the following fault plane solution: NP1: strike = 330°N, dip = 40°, slip = 120°; NP2: strike = 112°N, dip = 56°, slip = 67°. We prefer NP2 as the fault plane of S1, in conformity with the regional fault strike. The standard error of estimate of NP2 is 3.20. We have suggested earlier that this phase of energy was released about 5–6 s before the sub-event S2, from 33.6°N, 57.18°E, within the high angle reverse faults lying to the west of Tabas.

The asperities corresponding to the release of S4, S5 and S6 phases of energy, whose epicenters presumably are on the major surface rupture on which S3 epicenter is located, perhaps also occurred due to similar reverse thrust faulting on ESE–WNW striking, steeply dipping faults as S3.

We now attempt to estimate the source parameters of these sub-events by fitting appropriate ω^{-2} Brune source model spectra to the observed displacement amplitude spectra in the frequency band (0.1–0.2) Hz to (4.0–6.0) Hz at the three stations closest to the surface ruptures viz. Boshroyeh, Deyhook and Tabas (Fig. 6). Due to the possible low frequency cut and noise in the data, we find that it is difficult to get a reliable estimate of the most appropriate corner frequency (f_c) and zero spectral level (Ω_0) by direct visualization. Snoke (1987) has demonstrated with broadband data how the integral of the square of the ground velocity (J) and the cumulative displacement squared (K) can provide stable estimates of Ω_0 and f_c. He proposes the following formulae for estimating J and K.

$$J = 2\int_0^{\infty} |\omega U(\omega)|^2 \, \mathrm{d}\omega = \frac{2}{3}[\Omega_0\omega_1]^2 f_1 + 2\int_{f1}^{f2} |\omega U(\omega)|^2 \, \mathrm{d}\omega + 2|\omega_2 U(\omega_2)|^2 f_2 \qquad (2)$$

$$K = 2\int_0^{\infty} |\omega U(\omega)|^2 \, \mathrm{d}\omega = 2|U(\omega_1)|^2 f_1 + 2\int_{f1}^{f2} |\omega U(\omega)|^2 \mathrm{d}\omega + \frac{2}{3}[U(\omega_2)]^2 f_2 \qquad (3)$$

where $\omega = 2\pi f$; $U(\omega)$ is the far field displacement in the frequency domain which is assumed to have a constant amplitude for $f < f_1$ and a ω^{-2} fall-off for $f > f_2$. Then Ω_0 and f_c are given by the formulations (Snoke, 1987),

$$\Omega_0 = \left(\frac{4K^3}{J}\right)^{1/4} \quad \text{and} \quad f_c = \left(\frac{J}{4\pi^2 K}\right)^{1/2} \qquad (4)$$

For our study, for each sub-event case, we considered the observed displacement spectral data from the three stations Boshroyeh, Deyhook and Tabas in the frequency band (0.0–f_{max}) Hz and estimated J, K and subsequently Ω_0 and f_c at each station using Eq. (2) through (4). We note here (see Eqs. (2) and (3)) that while K is a measure of the power spectrum, J is a measure of the second moment (that is a measure of the standard error) of this power spectrum estimate. Hence, because all our calculations are conducted in the frequency band (0.0–f_{max}) Hz, we expect that our estimates of K integral will be smaller while the estimates of J integral will be larger than they really are. This implies that (see Eq. (4)), in every case, our calculated Ω_0 will always be an underestimate while the calculated f_c will be an overestimate of the true values. We confirmed this phenomenon by performing several tests with synthetic Brune displacement spectra on which different filters had been applied. For the sake of conciseness we do not discuss about those results in details here. Also, during our calculations with real data, we observed that for each sub-event case, at the three stations, these calculated Ω_0 values often showed large scatter but the calculated f_c values were quite stable, possibly because in the expression for Ω_0 the order of K is higher than that of J but in the expression for f_c these orders are same (see Eq. (4)).

For any particular sub-event case, at each of the three selected stations, we now use the calculated Ω_0 and the average of the calculated f_c (of the three stations), and adopt a sequential grid and search procedure to find the best-fit Brune ω^{-2} source model spectra (Brune, 1970, 1971) viz.

$$|U(f)| = \Omega_0 \, \mathrm{GS}(R) \exp\frac{(-\pi f t/Q_s)}{[1 + (f/f_c)^2]} \qquad (5)$$

Table 2
Estimated source parameters of the different subevents

Sub-event	Station	f_c (Hz)	M_0 (N m)	M_w	r (km)	E (erg)	$\Delta\sigma$ (bar)	D (m)	L (km)
S1	Tabas	0.19	0.01×10^{20}	5.97	3.9	2.4×10^{21}	7.4		
	Boshroyeh		0.01×10^{20}	5.97		2.4×10^{21}	7.4		
S2	Boshroyeh	0.10	0.70×10^{20}	7.20	7.5	1.7×10^{24}	75.5		
	Deyhook		0.90×10^{20}	7.27		2.8×10^{24}	95.3	25.5	18.80
	Tabas		1.02×10^{20}	7.30		3.6×10^{24}	108.0		
S3	Boshroyeh	0.10	0.12×10^{20}	6.69	7.5	5.0×10^{22}	12.7		
	Deyhook		0.30×10^{20}	6.95		3.1×10^{23}	31.8	8.49	18.80
	Tabas		0.20×10^{20}	6.83		1.4×10^{23}	21.1		
S4	Deyhook	0.14	0.04×10^{20}	6.37	5.3	1.5×10^{22}	11.7	2.27	13.29
S5/S6	Deyhook	0.14	0.04×10^{20}	6.37	5.3	1.5×10^{22}	11.7	2.27	13.29
S6/S5	Tabas	0.14	0.04×10^{20}	6.37	5.3	1.5×10^{22}	11.7		

to the corresponding observed SH-wave displacement spectra ($|U(f)|$) in the high fidelity frequency band viz. (0.1–0.2) Hz to (4.0–6.0) Hz (see Fig. 6). In this mathematical expression (5), f denotes the frequency expressed in Hz, t the travel time, GS(R) geometrical spreading, and R the source receiver distance. $GS(R) = R^{-1}$ for $R \leq R_y$ and $GS(R) = (RR_y)^{-0.5}$ for $R > R_y$. R_y may be taken as twice the thickness of crust (Herrmann and Kijko, 1983). We have taken R_y as 90 km (Berbarian, 1982). The term $\exp(-\pi ft/Q_S)$ accounts for the attenuation at high frequencies and describes inelastic attenuation of waves (e.g. Dainty, 1981; Fletcher, 1995).

The best-fit Brune model spectra (Fig. 6) can now be extrapolated to the long periods to provide the most appropriate estimates for the corner frequency (f_c) and the zero spectral level (Ω_0) for each case (Fig. 6). The seismic moment (M_0) is then given by $M_0 = F\Omega_0$ where $F = 4\pi\rho\beta^3/F_{SH}R_{\theta\phi}$ (Hanks and Thatcher, 1972), ρ is the density, β shear wave velocity, F_{SH} is the free surface effect (=2) and $R_{\theta\phi}$ is the radiation pattern calculated from the estimated fault plane solution. The moment magnitude (M_w) can be estimated from $M_w = (2/3)\log M_0 - 10.7$, where M_0 is expressed in dyne cm (Lay and Wallace, 1995). The radius of equivalent circular dislocation surface (r) is $r = 2.34\beta/2\pi f_c$, the energy radiated in the form of shear waves (E) is $E = (128\pi^3\rho\beta R^2\Omega_0^2 f_c^3)/15$ and the apparent stress drop ($\Delta\sigma$) is $\Delta\sigma = \mu E/M_0$, where μ is rigidity modulus (Hanks and Thatcher, 1972). We use these formulae to estimate the source parameters of the different sub-events (S1, S2, S3, S4, S5 and S6) (see Table 2).

We have assumed an average shear wave velocity (β) = 2.0 km/s, rigidity modulus (μ) = 2.0×10^{11} dynes/cm^2 and average density (ρ) = 1.5 g/cm^3 for our calculations. Although there is no detailed seismic velocity structure available for the Tabas region, Berbarian (1982) and Niazi and Shoja-Taheri (1985) inverted regional and local data to suggest a shear wave velocity of about 2 km/s in the shallow (<10 km) subsurface. The values assumed for μ and ρ are appropriate for limestone found in the local shallow subsurface and alluvial river deposits (see for example Jaeger, 1969). We note from our Brune model fits to the displacement spectra of S1, S2 and S3 (Fig. 6) that an average shear wave quality factor (Q_S) = 1200, 600 and 800 for the shallow subsurface near Tabas, Deyhook and Boshroyeh is quite appropriate.

So far, because of the paucity of accelerogram data, we have been unable to provide estimates of location parameters of S4, S5 and S6. But now with (i) these estimated values of Q_S and (ii) assuming equal corner frequencies (f_c) and zero spectral level (Ω_0) for these three sub-events, we fit appropriate Brune empirical spectra and thereby constrain their hypocentral distances (R) from Tabas and Deyhook (see Fig. 6). We find that for S4 (recorded at Deyhook) R = 30 km is most suitable. The most appropriate value of R for S5 (recorded at Deyhook) was found to be 66 km while for S6 (recorded at Tabas) it is found to be 40 km. We had earlier suggested from an analysis of the signatures of S4, S5 and S6 on the accelerograms (Figs. 1b and 2) that these sub-events appear to lie on the same major rupture as S3. Using this constraint and

the estimated values of R we now surmise (see Fig. 1a) that the locations of S5 and S6 epicenters possibly coincide. The indirect implication of this observation is that perhaps S5 and S6 in actuality represent the same sub-event.

5. Discussion

Shoja-Taheri and Anderson (1988) have identified signatures of four sub-events on the strong motion records at Tabas, Deyhook, Boshroyeh and Ferdows (S1, S2, S3 and S4 in their Fig. 4) and have suggested plausible epicentral locations for these sub-events (identified as 1–4 in their Fig. 6). The sub-events are seen more distinctly on their horizontal records from Deyhook (see their Fig. 4) and correspond to the phases marked as S2, S3, S4 and S5 on our Deyhook SH-wave accelerograms and velocity seismograms (see our Fig. 1b). Note that the location of the first sub-event S1 of Shoja-Taheri and Anderson (1988) (marked as 1 in their Fig. 6) coincides with the event location of Engdahl et al. (1998). This location is also our assumed location of S2 sub-event observed on our 'SH-wave' accelerograms and velocity seismograms, from where presumably the main phase of energy was released. Also our estimated location of the epicenter S3 (see Fig. 1a) is close, less than 10 km to the west of the location of corresponding sub-event 2 epicenter of Shoja-Taheri and Anderson (1988) (marked as 2 in their Fig. 6). Also our suggested locations of S4 and S5/S6 epicenters are slightly west of the locations of 3 and 4 of Shoja-Taheri and Anderson (1988).

Hartzell and Mendoza (1991) inverted simultaneously the strong motion records from Tabas, Deyhook and Boshroyeh and also WWSSN teleseismic records to provide details of the earthquake rupture history. Their numerical calculations could provide three well-resolved sources of energy. Of these, two main source regions of energy release, one around the hypocenter and the other 30 km NW of the hypocenter, extended from the surface to a depth of about 10 km. A third estimated source of energy release is from a region, at about 14 km depth, angled upwards towards Tabas town, approximately 50 km NW of the hypocenter. We may note here that our analysis estimates that (i) S3 hypocentre is located about 25 km NW of the estimated S2 hypocentre, (ii) both S2 and S3 hypocentres lie at a depth of 10 km approximately and (iii) S4 and S5/S6 also possibly lie to the NW of S3.

The source time function for the Tabas rupture process has been modeled by various inversion procedures. For example, Hartzell and Mendoza (1991) simultaneously inverted near field and far field P wave data from WWSSN networks to find the best fitting source-time function. Assuming a circular rupture and a constant propagating stress drop, they suggested either (i) a simple triangular source-time function with 0.7 s duration or (ii) a modified Kostrov source-time function with 2.9 s duration. They preferred the latter model because this gave an estimated moment and maximum displacement that was more consistent with the long-period surface waves and field observations. Walker et al. (2003), while ignoring the possibility that several asperities ruptured during the earthquake process, inverted long period P and SH wave data from WWSSN network to suggest a single, simple rupture event lasting for about 18 s. Obviously none of these simplified models are appropriate representation of the details of the complex Tabas rupture process.

We have estimated that the S3 phase of energy (corresponding to S2 phase of Shoja-Taheri and Anderson, 1988) was released about 9 s after the release of S2 phase of energy (corresponding to S1 phase of Shoja-Taheri and Anderson, 1988). Also our analysis of the Tabas, Deyhook and Boshroyeh 'SH-wave; accelerograms seem to suggest the occurrence of a sub event (designated S1 by us), about 5–6 s prior to the main phase of energy release (S2). Shoja-Taheri and Anderson (1988) have suggested, on the basis of an analysis of Deyhook records, that the last distinct phase of energy (designated S4 by them and as S5 by us) was released 22 ± 3 s after the first phase of energy (designated S1 by them and S2 by us) and also estimated that the rupture velocity is about 2.7 ± 2 km/s. The Deyhook transverse acceleration and velocity records (see Fig. 1b) show that the (S5–S2) shear wave arrival time is of the order of 36.4 s. We have suggested from the best-fit Brune ω^{-2} model spectrum that this sub-event is located about 66 km away from Deyhook, which, for a rupture velocity of 2.7 km/s, implies that S5 phase of energy was released approximately 20 s after the release of S2 phase of energy, a result that is in conformity to Shoja-Taheri and Anderson (1988)'s result. Again, from Deyhook transverse acceleration and velocity records (see Fig. 1b) we find that (S4–S2) shear

wave arrival time is of the order of 20.0 s. For a rupture velocity of 2.7 ± 2 km/s and a hypocentral distance of 30 km (estimated from the best-fit Brune ω^{-2} model spectrum), this suggests that possibly S4 phase of energy was released approximately 16.8 ± 0.8 s after the release of S2 phase of energy.

The various analysis of the Tabas earthquake fault, based on a single point source representation and teleseismic data, obtains strike, dip and slip of around 332°, 30° and 110°, respectively (Berbarian et al., (1979); Niazi and Kanamori, (1981) and CMT solution). However, Walker et al., (2003) used regional and teleseismic data jointly to obtain strike, dip and slip of around 355°, 16° and 155°, respectively. In our study, we have estimated the strike, dip and slip for the two larger sub-events (S2 and S3) to be approximately 110°, 83° and 75°, respectively, which are in closer conformity to the estimates given by Berbarian et al., (1979), Niazi and Kanamori, (1981) and CMT solution. Also our estimated strikes of the fault planes of these two sub-events are sub-parallel to the regional strike of exposed faults in the area. We note that the alternate nodal planes have strikes in a nearly N–S direction.

In inversion procedures based on teleseismic data, the earthquake has been modeled as a point source and with a single simple rupture process. Hence the ensuing results provide a model for the overall slip on the Tabas causative fault. On the other hand, analysis of near field, high frequency and higher near source spatial coverage data provide detailed information on the roughness of the failure process over the fault plane by highlighting the jittering effects in the total slip process related to asperity failure. In this study several asperities on the causative fault have been identified. Inversion of near field data and assuming a double couple source model shows that the (preferred) fault planes of the two larger asperities are both steeply dipping (dip = 83°), generally oriented ESE–WNW (strike = 110° and 107°) and exhibit similar predominantly reverse thrust motion along with prominent left-lateral strike slip component (slip = 75.0°). We have earlier surmised that the asperities corresponding to the two/three other smaller sub-events also have similar orientation and slip direction.

Our analysis of the predominantly high frequency (0.2 Hz < f < 6.0 Hz), near field data has thus provided detailed information about the different aspects of the complex rupture process that occurred in different sections of the Tabas thrust fault system. It is surmised that during the Tabas rupture process several sub-events occurred at shallow depths, on steeply dipping ESE–WNW striking sub-faults, due to reverse thrust faulting along with some major strike slip component. These results are consistent with the complex geological structure of the area that is demonstrated by the series of exposed traces of faults that are often offset at a number of places. Also we may note here Berbarian (1982)'s remarks on the basis of a detailed analysis of some major aftershock sequences of the Tabas earthquake that "The most striking feature of this faulting is that apparently several listric thrust planes were involved."

Because of the noise and deficiency of low frequency components in the data, there is some scatter in our estimated M_0 for the different sub-events. However, considering (i) the reported seismic moment (M_0) and moment magnitude (M_w) of the Tabas event viz. $M_0 = 1.32 \times 10^{20}$ N m and $M_w = 7.4$ and (ii) our estimated seismic moments and moment magnitudes of the five sub-events (see Table 2), we note that the total seismic energy released during the entire earthquake process is equivalent to that released during the occurrence of these five more significant sub-events in totality. Also note in Table 2 that our empirical estimates of the shear wave energy radiated by the different sub-events are generally higher than those estimated directly from seismograms by Shoja-Taheri and Anderson (1988). Also while their energy estimates at Deyhook are suggested to be equal, our estimates are varied. Further our values are on a higher side than those predicted by the well-known relation $\log E = 11.8 + 1.5M_w$. Our estimates of the stress that caused the seismic radiation during most of the sub-events (presumably the apparent stress drop) are generally less than 30 bar. However for S2 sub-event, the main energy released is very high, of the order of 100 bar at Deyhook and Tabas. Of course the Brune model estimate for the stress drop has often been found to be unstable, especially in case of complex rupture processes (for example, see Snoke, 1987). However, we suggest that in the region surrounding the S2 asperity, on the heterogeneous causative fault plane, where fracture was initially resisted, there was possibly a large increase of dynamic stress that eventually caused breakage of this strong patch and, as a result, a localized extremely high stress drop occurred.

We have noted earlier that Tabas and Boshroyeh are located on either side of the major surface ruptures, at approximately equal epicentral distance from the source of main energy release. This information along with the regional seismic velocity model parameters (Berbarian, 1982; Niazi and Shoja-Taheri, 1985) suggests that the earlier arriving SH-waves at both these stations are direct waves. The estimated values of the average shear wave quality factor (Q_S) for the subsurface near Tabas and Boshroyeh (viz. 1200 and 800, respectively) then implies that the attenuation time, t^* (Cormier, 1982) within the shallow subsurface rocks near Tabas is about 0.6 times less than that near Boshroyeh. In shallow rocks, Q_S and hence t^* are generally independent of frequency (f). Anderson and Gough (1984) have reasoned that for $f > f_E$, when the spectral decay parameter κ is also independent of frequency, the effect of attenuation on the shape of the ω^{-2}-source model acceleration spectrum in terms of t^* and κ are equivalent. In other words, our average Q_S (and t^*) estimates suggest that the decay parameter κ should also be much less in the shallow rocks near Tabas than in those near Boshroyeh. This suggestion is in conformity with Shoja-Taheri and Anderson (1988)'s direct estimates of κ from the horizontal and vertical acceleration records of these stations. Further Anderson and Gough (1984) have suggested that $(f_{max} - f_E)$ is inversely proportional to κ. We note that while f_{max} is generally of the order of 7 Hz at both Tabas and Boshroyeh (see Figs. 3 and 4), f_E at the former station is about 3–4 Hz while that at the latter is about 5–6 Hz. This further evinces that the decay parameter κ near Tabas is less than that near Boshroyeh.

To investigate the interdependence of the various faulting parameters estimated in this study, the modeled Brune displacement spectral density for the S2, S3, S4 and S5 phases of energy observed at Deyhook are plotted as a function of frequency (Fig. 7). Note that the estimated corner frequencies lie on a straight line suggesting a consistency in the scaling law of the seismic spectrum here.

We now investigate how the source parameters scale for the Tabas earthquake sub-events. Note that M_0 and corresponding f_c values for the sub-events, estimated from the accelerograms recorded at Deyhook (see Table 2) suggest that generally f_c is inversely proportional to $\sqrt[3]{M_0}$. Further, assuming a fault aspect ratio of 2, the average length (L) of these four asperities

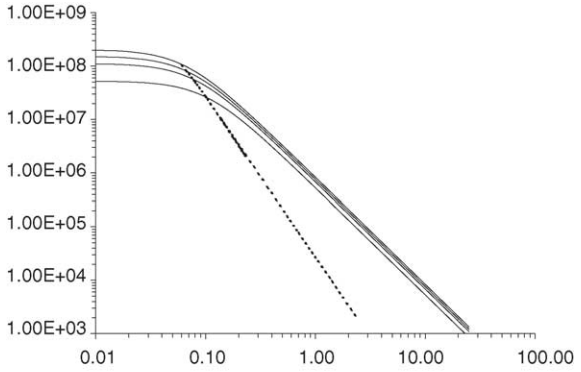

Fig. 7. The source spectra for ground displacement at Deyhook for the sub-events S2, S3, S4 and S5. The broken line shows that the corner frequency increases with decrease in the seismic moments of these events. This suggests the consistency in the scaling law of the seismic spectrum here.

have been estimated at Deyhook (Table 2). Note that $\log L$ is directly proportional to $\log M_0$. This suggests that there was constant stress drop during occurrence of these sub-events. Further the average slip D caused during the rupture of these four asperities, calculated from M_0, μ and area of dislocation surface (πr^2) (e.g. Aki and Richards, 1980; Lay and Wallace, 1995) are tabulated in Table 2. From the ratio D/L for the four sub events, a uniform strain drop of the order of 10^{-4} is predicted. The possibility that shallow earthquakes in typical continental conditions involve strains of the order of 10^{-5} to 10^{-4} has often been mentioned in literature (Lay and Wallace, 1995). Such a pattern of constancy in the estimated stress/strain drop indicates the self-similarity between earthquakes of the region.

The observed peak ground acceleration (PGA) values are tabulated in Table 1. Several factors, e.g. local topography, seismic source, propagation path, local site conditions are generally expected to influence PGA. Comparison of the recorded PGA at the various accelerograph stations reveals the following pattern. The vertical PGA is always smaller than the horizontal PGA. The Tabas site lies closest to the fault outcrop, towards the northern, terminal end of the north/northwestward propagating causative rupture; as a result the observed horizontal PGA is largest there. The next largest value is at Deyhook, lying at the southern end of the rupture from where the energy release was shown to have initiated. The recorded

PGA at Tabas is amplified by a factor of about 3 in comparison to that at Deyhook due to local site effects. While Deyhook lies over thin sediments that are emplaced on the flanks of the limestone hills where the accelerograph station is located, Tabas sits on a thick accumulation of soft sediments. According to Shoja-Taheri and Anderson (1988) the rupture propagated in the overlying sediments with a very high velocity, which also will cause the large amplification of ground acceleration at Tabas. The PGA values at Boshroyeh, Ferdows and Bajestan, lying within heavily deformed alluvial and fluvial soil, generally to the north east of the (north westerly propagating) rupture direction and at greater distance from it, are comparable and are all much smaller than those recorded at Tabas and Deyhook. The PGA values at Sedeh and Kashmar are smallest because these stations lie at greatest distance from the rupture zone, to the east and north east of the northwesterly propagating rupture, respectively.

Niazi and Bozorgnia (1992) have proposed attenuation relations for the horizontal and vertical PGA within the Alborz mountain regions. Sarkar et al. (2003) found support for one of those relations from the horizontal PGA recorded in that region during the 1990 Rudbar earthquake. In Fig. 8, we examine that particular attenuation relation and also one that was proposed by Abrahamson and Litehiser (1989) from worldwide data with the PGA recorded during the Tabas earthquake. It is observed that the predicted values from Abrahamson and Litehiser (1989)'s relation are always far lower, by an order of 0.3 g or so. In fact the observed PGA values are slightly higher than those predicted by Niazi and Bozorgnia (1992) also, at least for the nearer stations.

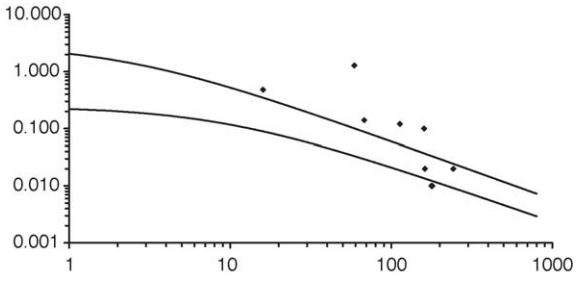

Fig. 8. The variation of attenuation of horizontal peak ground accelerations (in g) with hypocentral distance. The black dots denote the observed values at the nine stations. Graphs 1 and 2 are from attenuation relations of Abrahamson and Litehiser (1989) and Niazi and Bozorgnia (1992), respectively.

6. Conclusions

The following conclusions emerge from this study:

1. The 'SH-wave' accelerograms, derived from the observed horizontal accelerograms, exhibit distinct signatures of high frequency energy released from four (or possibly five) asperities on the Tabas fault system during the unilateral propagation of rupture in a southeast-to-northwest direction.
2. The first sub-event is a foreshock that occurred about 5–6 s prior to the main energy release. A smaller sub-event, located to the west of the main sub-event epicenter, followed about 9 s after. Two (or possibly three) smaller sub-events, whose epicenters are also located to the west of the main sub-event epicenter, follow about 20 s or so after these events. The last event perhaps corresponds to the termination of the fault process.
3. The asperity corresponding to the foreshock is interpreted to be located to the east of Tabas, within the high angle reverse faults which lie between Tabas and Boshroyeh. The main asperity corresponding to the main release of energy lies at the southern end of the fault system, close to Deyhook. The sub-event corresponding to next phase of energy release is placed on the NW–SE trending main fault segment, approximately midway between Tabas and Deyhook. The two/three smaller sub-events are surmised to be also located on the same segment. It seems plausible that while one of these lies closer to Deyhook, at the southeastern end of the fault segment, the other is closer to Tabas, at its northwestern end.
4. The preferred fault planes corresponding to the main and the following sub events strike ESE–WNW, dip at steep angles and exhibit predominantly reverse thrust motion along with some left-lateral strike-slip component. Such a slip process is in conformity with a northwesterly propagating rupture that initiated at the base of a listric thrust fault. The foreshock occurred due to reverse thrusting on a steeply dipping, NNW–SSE striking fault.
5. The displacement spectra fit Brune ω^{-2} source model well. Using suitable model fit with appropriate zero spectral level (Ω_0), corner frequency (f_c) and local Q_S values, the seismic moment, moment magnitude, rupture size, radiated shear wave energy

and average stress drop of all the asperities have been estimated.
6. The sub-events exhibit self-similarity.
7. The pattern of observed PGA values are consistent with a northwesterly-directed unilateral rupture propagation process. These also exhibit distinct effects of the local geological site conditions.
8. The attenuation relation proposed by Niazi and Bozorgnia (1992) for the Alborz region fairly predicts the observed PGA data.
9. The average shear quality factor Q_S is estimated to lie between 600 and 1200, depending on local site geology of the path.

Acknowledgement

We are grateful to Building and Housing Research Center, Islamic Republic of Iran for providing the strong motion data we analyze here in this study. We appreciate the constructive comments of the referees that have led to considerable improvement in this contribution. IS, VS and HH thank their respective organizations for support during this research work.

References

Abrahamson, N.A., Litehiser, J.J., 1989. Attenuation of vertical peak acceleration. Bull. Seism. Soc. Am. 79, 549–580.
Aki, K., Richards, P.G., 1980. Quantitative Seismology, vol. 1. Freeman, San Francisco, CA.
Anderson, J.G., Gough, S.E., 1984. A model for the shape of the Fourier amplitude spectrum of acceleration at high frequencies. Bull. Seism. Soc. Am. 74, 1969–1993.
Berbarian, M., Asuder, I., Bilham, R.G., Scholz, C.H., Soufleris, C., 1979. Mechanism of the main shock and the aftershock study of the Tabas-e-Golshan (Iran) earthquake of September 16, 1978: a preliminary report. Bull. Seism. Soc. Am. 69, 1851–1859.
Berbarian, M., 1979a. Evaluation of the instrumental and relocated epicenters of the Iranian earthquakes. Geophys. J. R. Astr. Soc. 58, 625–630.
Berbarian, M., 1979b. Earthquake faulting and bedding thrust associated with the Tabas-e-Golshan (Iran) earthquake of September 16, 1978. Bull. Seism. Soc. Am. 69, 1861–1887.
Berbarian, M., 1982. Aftershock tectonics of the 1978 Tabas-e-Golshan (Iran) earthquake sequence: a documented active 'thin- and thick-skinned tectonic' case. Geophys. J. R. Astr. Soc. 68, 499–530.
Brune, J.N., 1970. Tectonic stress and the spectra of seismic shear waves from earthquakes. J. Geophys. Res. 75, 4997–5009.
Brune, J.N., 1971. Correction. J. Geophys. Res. 76, 5002.
Campos, J., Madariaga, R., Nabalek, J., Bukchin, B.G., Deschamps, A., 1994. Faulting process of the 1990, June 20 Iran earthquake from broad-band records. Geophys. J. Int. 118, 31–46.
Cormier, V.F., 1982. The effect of attenuation on seismic body waves. Bull. Seism. Soc. Am. 72, S169–S200.
Dainty, A.M., 1981. A scattering model to explain seismic Q observations in the lithosphere between 1 and 30 Hz. Geophys. Res. Lett. 8, 1126–1128.
Engdahl, E.R., van der Hilst, R., Buland, R., 1998. Global teleseismic earthquake relocation with improved travel times and procedures for depth determination. Bull. Seism. Soc. Am. 88, 722–743.
Fletcher, J.B., 1995. Source parameters and crustal Q for four earthquakes in South Carolina. Seism. Res. Lett. 66, 44–58.
Hamzehloo, H., Sarkar, I., Chander, R., 1997. Analysis of some aftershocks of the Rudbar earthquake of 1990 using master event technique. Bull. Indian Soc. Earthq. Technol. 33, 1–16.
Hanks, T.C., Thatcher, W., 1972. A graphical representation of seismic source parameters. J. Geophys. Res. 77, 4393–4405.
Hartzell, S., Mendoza, C., 1991. Application of an iterative least-squares waveform inversion of strong-motion and teleseismic records to the 1978 Tabas, Iran, earthquake. Bull. Seism. Soc. Am. 81, 305–331.
Haskell, N.A., 1960. Crustal reflection of plane SH waves. J. Geophys. Res. 65, 4147–4150.
Herrmann, R.B., Kijko, A., 1983. Modelling some empirical vertical component L_g relations. Bull. Seism. Soc. Am. 73, 157–171.
Jaeger, J.C., 1969. Elasticity, Fracture and Flow. Methuen and Company, London.
Kanamori, H., Stewart, G.S., 1978. Seismological aspects of the Guatemala earthquake of February 4, 1976. J. Geophys. Res. 83, 3424–3427.
Kumar, D., Sarkar, I., Sriram, V., Khattri, K.N., 2005. Estimation of the source parameters of the Himalaya earthquake of October 19, 1991, average effective shear wave attenuation parameter and local site effects from accelerograms. Tectonophysics (under review).
Lay, T., Wallace, T.C., 1995. Modern Global Seismology. Academic Press, San Diego, California.
Mendoza, C., Hartzell, S., 1989. Slip distribution of the 19 September 1985 Michoacan, Mexico, earthquake: near-source and teleseismic constraints. Bull. Seism. Soc. Am. 79, 655–669.
Mohajer-Ashjai, A., Nowroozi, A.A., 1979. The Tabas earthquake of September 16, 1979 in east-central Iran, a preliminary report. Geophys. Res. Lett. 6, 689–692.
Niazi, M., Kanamori, H., 1981. Source parameters of 1978 Tabas and 1979 Qainat, Iran earthquakes from long-period surface waves. Bull. Seism. Soc. Am. 71, 1201–1213.
Niazi, M., Shoja-Taheri, J., 1985. Source geometry and mechanism of 1978 Tabas, Iran earthquake from well located aftershocks. Tectonophysics 115, 61–68.
Niazi, M., Bozorgnia, Y., 1992. The 1990 Manjil, Iran earthquake: geology and seismological overview, PGA attenuation and observed damage. Bull. Seism. Soc. Am. 82, 774–799.
Sarkar, I., Chander, R., Chatterjee, D., 1995. On the aftershock sequence of a 4.6 m_b earthquake of the Garhwal Himalaya. Proc. Indian Acad. Sci. (Earth Planet. Sci.) 104, 683–691.

Sarkar, I., Hamzehloo, H., Khattri, K.N., 2003. Estimation of causative fault parameters of the Rudbar earthquake of June 20, 1990 from near field SH-wave data. Tectonophysics 364, 55–70.

Shoja-Taheri, S., Anderson, J.G., 1988. The 1978 Tabas, Iran, earthquake: an interpretation of the strong motion records. Bull. Seism. Soc. Am. 78, 142–171.

Snoke, J.A., 1987. Stable determination of (Brune) stress drops. Bull. Seism. Soc. Am. 77, 530–538.

Walker, R., Jackson, J., Baker, C., 2003. Surface expression of thrust faulting in eastern Iran: source parameters and surface deformation of the 1978 Tabas and 1968 Ferdows earthquake sequences. Geophys. J. Int. 152, 749–765.

Wyss, M., Brune, J.N., 1967. The Alaska earthquake of 28 March 1964: a complex multiple rupture. Bull. Seism. Soc. Am. 57, 1017–1023.